SCIENCE CHINA
Physics, Mechanics & Astronomy

• Article •

May 2019 Vol. 62 No. 5: 957412
https://doi.org/10.1007/s11433-018-9362-x

Structure, charge transfer, and superconductivity of *M*-doped phenanthrene (*M* = Al, Ga, and In): A comparative study of K-doped cases

Hai-Yan Lv[1,2], Guo-Hua Zhong[1,3*], Ming Chen[1*], Chun-Lei Yang[1], Xiao-Jia Chen[4], and Hai-Qing Lin[3]

[1] *Shenzhen Institutes of Advanced Technology, Chinese Academy of Sciences, Shenzhen 518055, China;*
[2] *Nano Science and Technology Institute, University of Science and Technology of China, Suzhou 215123, China;*
[3] *Beijing Computational Science Research Center, Beijing 100193, China;*
[4] *Center for High Pressure Science and Technology Advanced Research, Shanghai 201203, China*

Received December 29, 2018; accepted January 28, 2019; published online March 7, 2019

Aromatic hydrocarbons doped with K have been shown to be potential high-temperature superconductors. To investigate the doping effects of trivalent metals (Al, Ga, and In) that have a smaller radii than K, we studied the crystal structure, stability, charge transfer, band structure, and superconductivity of trivalent metal-doped phenanthrene via first-principles calculations. Doping with Al/Ga/In considerably differs from doping with K and cannot be simply regarded as a linear developmental change in the structural and electronic characteristics caused by a change in the valence electron numbers. Al/Ga/In atoms are difficult to dope into the intralayer region, and the charge transfer is close to zero, which is far less than the effect of K doping. We found that the metallization of the Al/Ga/In-doped system originates from the formation of gap states instead of charge transfer. The weak superconductivity obtained in the Al/Ga/In-doped system is also different from the K-doped system. These results are helpful in terms of understanding the structure and superconductivity of metal-doped aromatic superconductors.

phenanthrene, aromatic hydrocarbons, trivalent metals, charge transfer, superconductivity

PACS number(s): 74.70.Kn, 61.66.Hq, 74.25.Jb, 71.20.-b

Citation: H.-Y. Lv, G.-H. Zhong, M. Chen, C.-L. Yang, X.-J. Chen, and H.-Q. Lin, Structure, charge transfer, and superconductivity of *M*-doped phenanthrene (*M* = Al, Ga, and In): A comparative study of K-doped cases, Sci. China-Phys. Mech. Astron. **62**, 957412 (2019), https://doi.org/10.1007/s11433-018-9362-x

1 Introduction

Metal-doped aromatic compounds are considered potential high-temperature superconductors because the electrons can interact with a much higher excitation energy than the phonon energy in these materials [1-3]. In 2010, Mitsuhashi et al. [4] observed a superconducting transition in K_x picene with a critical temperature (T_c) of up to 18 K from 7 K. In 2011, Kubozono et al. [5] reported the superconductivity in K_x coronene, and four superconducting phases with T_c values of 3.5, 7, 11, and 15 K were found in this sample. Subsequently, the superconductivity was also discovered in K_x phenanthrene ($T_c \sim 5$ K) [6,7] and K_x dibenzopentacene ($T_c \sim 5$, 7.4, 25, and 33 K) [8], respectively. As a result, we observed that the highest value of T_c increases with the size of the organic molecule, such as from 5 K of phenanthrene to 18 K of picene and then to 33 K of 1,2;8,9-dibenzopentacene [4, 6-8]. It seems that a higher T_c may be obtained by adjusting the number of benzene rings and their arrangement. Thus, these studies opened a new avenue in the quest for high-temperature su-

*Corresponding authors (Guo-Hua Zhong, email: gh.zhong@siat.ac.cn; Ming Chen, email: ming.chen2@siat.ac.cn)

perconductors. Most recently, the observations of superconductivities in K-doped *p*-biphenyl [9], *p*-terphenyl [10-16], *p*-quaterphenyl [14, 17], and *p*-quinquephenyl [18] further confirmed the feasibility of Ginzburg and Little's idea. Superconductivities above 120 K have been observed in both K-doped *p*-terphenyl and *p*-quaterphenyl [12, 13, 17].

Similar to other charge-transfer-type superconductors [19-22], the charge transfer also plays a key role in these aromatic hydrocarbon superconductors. The transferred charge is donated by metals, such as K, Rb, and Cs. From previous studies, the alkali metal K with one valence electron has been found to be perfect for intercalating into aromatic hydrocarbons. This is mainly due to the K metal's low melting point at ~ 30°C, which implies that it can react with aromatic hydrocarbons at lower temperatures. Although we theoretically pointed out that a low-T_c phase should correspond to two-electron doping, and a high-T_c phase possibly results from higher doping levels, such as the three-electron doping, the mole ratio between K and the organic molecule in the experimental process is often approximately 3:1. Could one atom of divalent metals (Mg, Ca, Sr, and Ba) or one atom of trivalent metals (Al, Ga, and In) with multiple valence electrons replace K to provide the charge? Considering the melting point, all of the Mg, Ca, Sr, and Ba metals have values larger than 650°C, which indicates the difficulty of the solid state reaction between divalent metals and organic molecules. Indeed, Ba intercalating into phenanthrene leads to the formation of BaC_2 carbide or amorphous carbon [23]. In contrast, trivalent metals have a lower melting point; in particular, 30°C for Ga and 157°C for In. Moreover, Al, Ga, and In, have smaller radii than K. This means that the trivalent metals are able to replace K as an electron supply source and will only request one trivalent atom for every organic molecule.

Moreover, the reaction temperature of interpolating three K atoms into an organic compound is difficult to control, which makes the experimental preparation challenging. Hence, we envision whether the same effect can be obtained by replacing three K atoms with one trivalent atom. What is the structure, stability, charge transfer, and electronic properties after doping? These are still unknown. Therefore, in this work, we conducted a related study using the trivalent metal M (M = Al, Ga, and In)-doped phenanthrene ($MC_{14}H_{10}$) as an exampleand compared it with the K-doped case ($K_xC_{14}H_{10}$).

2 Computational methods

For $MC_{14}H_{10}$, we used CALYPSO software [24, 25] based on particle swarm optimization to search for doping structures. Within the framework of density functional theory, the Vienna *ab initio* simulation package (VASP) [26, 27] based on the projector augmented wave method was employed to optimize the lattice parameters and calculate the electronic structures. The generalized gradient approximation (GGA) of the exchange correlation functional (Perdew-Burke-Ernzerh of 96, PBE) was adopted [28]. Considering the non-local interactions, we added the correction of van der Waals (vdW) in the version of vdW-DF2 in the calculations [29]. The necessity of the vdW-DF2 functional was confirmed in our previous studies [9,17,18,30-32]. An energy cutoff of 600 eV was adopted. Structural optimization used a conjugate-gradient algorithm, and the k-point of the Brillouin zone was a 0.04 $Å^{-1}$ interval distribution of Monkhorst-Pack. The k-point interval of the total energy self-consistent calculation was 0.02 $Å^{-1}$. The energy convergence standard was 10^{-6} eV. The convergence criterion of the force was 10^{-3} eV/Å.

To predict the possible superconductivity, at the same time, the electron-phonon interaction was calculated using the density functional perturbation theory [33] and the Troullier-Martins norm-conserving potentials [34], as implemented in the QUANTUM-ESPRESSO (QE) code [35, 36]. The cutoff energies of 80 and 600 Ry were used for wave functions and charge densities, respectively. A $4 \times 4 \times 4$ Monkhorst-Pack k-point grid with Gaussian smearing of 0.003 Ry was used for the electron-phonon interaction matrix element calculation at a $2 \times 2 \times 2$ q-point mesh. In both VASP and QE codes, the same functional was selected. Forces and stresses for the converged structures were optimized and checked to be within the error allowance of the VASP and QE codes.

3 Results and discussion

3.1 Crystal structures and stability

Trivalent metal atoms were intercalated into pristine phenanthrene crystals to achieve different doping configurations by changing the positions of the trivalent atoms. Although there are two organic molecules in a unit cell, a phase transition occurs from pristine to doped phenanthrene. After the optimizations, we found that the structure of $MC_{14}H_{10}$ with the $P1$ space group was the most stable and $MC_{14}H_{10}$ has similar structural characteristics for each M dopant. To visually view these doped structures, we showed the most stable and two typical metastable structures for each M dopant in Figure 1. Additionally, to check the stability of these configurations, we calculated the formation energy for each configuration by the formula $E_f = E_{doped} - E_{pristine} - nE_M$, where E_{doped} and $E_{pristine}$ are the total energies of the doped and pristine systems, respectively, and E_M is the energy of a single atom

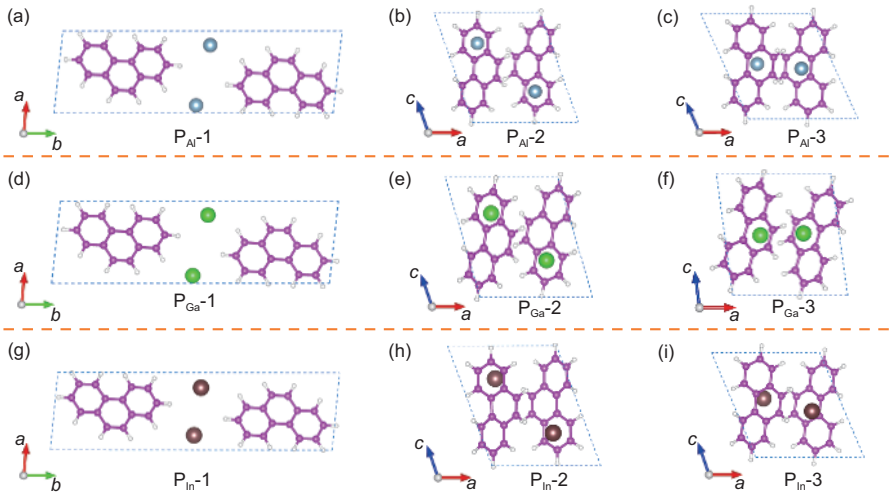

Figure 1 (Color online) Optimized crystal structures of the trivalent-metal-doped phenanthrene. (a), (b), and (c) correspond to the Al-doped phenanthrene (P_{Al}); (d), (e), and (f) correspond to the Ga-doped phenanthrene (P_{Ga}); (g), (h), and (j) correspond to the In-doped phenanthrene (P_{In}). The most stable configuration is marked by P_M-1 (M = Al, Ga, and In), while the two metastable structures are marked as P_M-2 and P_M-3, respectively. Light blue, green, and brown balls represent Al, Ga, and In atoms, respectively.

in metal M. As shown in Figure 1(a), (d), and (g), viewing along the c-direction, the feature of the most stable structures (P_{Al}-1, P_{Ga}-1, and P_{In}-1) is that the trivalent metal overflows from the molecular layer into the interlayer region. In contrast, when the trivalent metal atoms move into the intralayer region, the structure becomes metastable with $P2_1$ symmetry. As listed in Table 1, the formation energy will increase to 2.030 eV for P_{Al}-2, 1.468 eV for P_{Ga}-2, and 1.405 eV for P_{In}-2, when Al, Ga, or In atoms move into the intralayer region at both ends of the organic molecule as shown in Figure 1(b), (e), and (h). When the Al, Ga, or In atoms further move to the center from the ends of the organic molecule, as shown in Figure 1(c), (f), and (i), the structure is still metastable. As shown in Table 1, although the formation energy slightly decreases, the formation energies of P_{Al}-3, P_{Ga}-3, and P_{In}-3 are still much higher than that of the most stable structure.

For comparison, we also present the most stable and metastable structures of $K_xC_{14}H_{10}$ in Figure 2. Three kinds of doping levels of x = 1, 2, and 3 were considered for $K_xC_{14}H_{10}$ containing two organic molecules in the unit cell. The experimental results indicate that no phase transition appears when K metal is doped into the phenanthrene crystal and it retains the $P2_1$ symmetry [6, 7]. According to previous studies [37], the most stable structures of $K_xC_{14}H_{10}$ include K atoms staying in the intralayer region formed via organic molecules, as P_{K1}-1, P_{K2}-1, and P_{K3}-1, which are shown in Figure 2(a), (d), and (g), respectively. In contrast to the intercalation by a single trivalent metal atom, for $K_1C_{14}H_{10}$, K atoms are localized at the center of the organic molecule along the b-direction. For $K_2C_{14}H_{10}$ and $K_3C_{14}H_{10}$, K atoms tend to distribute in the intralayer region in the most stable structures. Combining the structures shown in Figure 2 and the formation energies listed in Table 1, for metastable structures, clearly, the movement of K atoms into the interlayer region results in an increase in formation energy for every doping level.

Table 1 Formation energy (E_f) and transferred charge (Δ_q) from M to the phenanthrene molecule for every metal-doped structure

Structure	E_f (eV/f.u.)	Δ_q (e/f.u.)
P_{K1}-1	–0.280	0.83
P_{K1}-2	1.324	0.77
P_{K1}-3	2.643	0.78
P_{K2}-1	–0.600	1.64
P_{K2}-2	1.045	1.39
P_{K2}-3	2.017	1.18
P_{K3}-1	–0.360	2.37
P_{K3}-2	1.572	1.93
P_{K3}-3	2.893	1.69
P_{Al}-1	0.922	0.07
P_{Al}-2	2.030	0.56
P_{Al}-3	1.828	0.63
P_{Ga}-1	0.588	0.06
P_{Ga}-2	1.468	0.44
P_{Ga}-3	1.329	0.50
P_{In}-1	0.553	0.06
P_{In}-2	1.405	0.49
P_{In}-3	1.336	0.51

As a result, the K atoms can distribute in the intralayer region for K-doped phenanthrene. Similar phenomena of K atoms easily staying in the intralayer region of the organic molecules have also been observed in other K-doped aromatic hydrocarbons [9, 17, 18, 30-32]. Conversely, the trivalent metal atoms must move into the interlayer region for $MC_{14}H_{10}$. Additionally, based on the formation energy of the most stable structures shown in Table 1, phenanthrene doped by a trivalent metal results in a positive value, which indicates that the stability of $MC_{14}H_{10}$ is inferior to that of $K_xC_{14}H_{10}$.

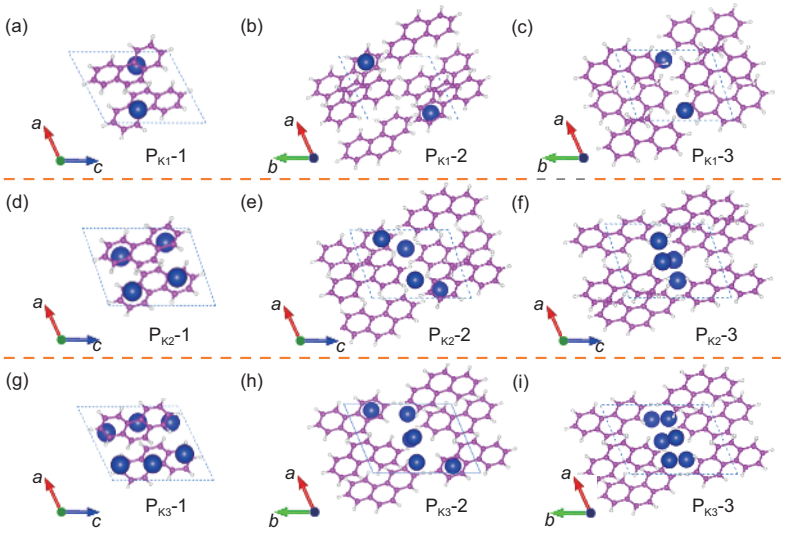

Figure 2 (Color online) Optimized crystal structures of the K-doped phenanthrene. (a), (b), and (c) correspond to K_1 phenanthrene (P_{K1}); (d), (e), and (f) correspond to K_2 phenanthrene (P_{K2}); (g), (h), and (j) correspond to K_3 phenanthrene (P_{K3}). The most stable configuration is marked as P_{Kx}-1, while the two metastable structures are marked as P_{Kx}-2 and P_{Kx}-3, respectively. Blue balls represent K atoms.

Hence, trivalent metal atoms are not easy to intercalate into the intralayer region of phenanthrene molecules, although Al, Ga, and In have smaller radii than the K atom. Table 2 lists the crystal lattice parameters of the pristine phenanthrene and the most stable structures of the K-doped and *M*-doped phenanthrene. Whether it is K, Al, Ga or In, the doping makes the volume larger. The volume induced by the trivalent metal doping is larger than that of $K_1C_{14}H_{10}$ but less than that of $K_3C_{14}H_{10}$.

3.2 Charger transfer and band structure

To further investigate the difference between the trivalent metals and the K metal for doping, the charge transfer was calculated and is presented in Table 1 for several typical structures. As shown in Table 1, when the doping concentrations of K are 1, 2, and 3, the charge transfer numbers from metal to organic molecules in the most stable configurations are 0.83, 1.64, and 2.37 e/f.u., respectively. All are close to doping concentration and are a multiple of 0.8 e/f.u.. However, the charge transfer numbers of the most stable structure of Al, Ga, and In atoms doped in phenanthrene are only 0.07, 0.06, and 0.06 e/f.u., respectively, and charge transfer is almost negligible. The result exhibits the obvious distinction between K and Al/Ga/In dopants regarding charge transfer. Because of the different structures caused by K and Al/Ga/In doping, we considered whether the difference in doping configurations causes a huge gap in charge transfer. Because the doping of K atoms enters the inner region of the organic molecule, we also selected the metastable structures of Al/Ga/In entering the interior of the phenanthrene. The calculated charge transfer data is provided in Table 1. When the trivalent atom was inserted into the molecular layer, the number of charge transfers increased, which indicates that the structural change influences the charge transfer; however, it was still much smaller than 3e, which did not reach the result of our original conjecture. When the K atoms were located in the interlayer region of the organic molecules, the number of charge transfer only slightly decreased, which is exactly the opposite of the trivalent metal doping. An obvious charger transfer was also obtained for K-doped other aromatic hydrocarbons [9, 17, 18, 32]. By analyzing charge transfer and stability in combination, we concluded that the trivalent metal-doped phenanthrene hardly underwent charge transfer.

In K-doped aromatic hydrocarbons, the transition from insulator to metal is mainly induced by charge transfer. Electrons from the metal fill the empty conduction bands, which results in metallization. The electronic bands exhibit a quasi-rigid feature. Thus, electronic band structures still retain part of their characteristics before doping. We call most K-doped aromatic hydrocarbons charge transfer superconductors. However, the charger transfer is absent in $MC_{14}H_{10}$. To examine the electronic properties, we calculated the DOS and band structures along high-symmetry *k*-point paths in the Brillouin zone of $MC_{14}H_{10}$, which are shown in Figures 3 and 4, respectively. Interestingly, $MC_{14}H_{10}$ exhibits metallic behavior. In most stable structures, such as P_{Al}-1, P_{Ga}-1, and P_{Ga}-1, as shown in Figure 3, the DOS values at the Fermi level are 0.3, 1.7, and 2.2 states/eV/f.u., respectively, and there is a visible plateau effect near the Fermi level in P_{Al}-1 and P_{Ga}-1. From the band structures shown in Figure 4, P_{Al}-1 has a similar band feature to P_{Ga}-1, exhibiting two dimensional characteristics along the Γ-*Y*-*A*-*B* and

Table 2 Optimized crystal lattice parameters of the most stable structures for K-doped and *M*-doped phenanthrene compared with pristine phenanthrene

Structure	Space group	*a* (Å)	*b* (Å)	*c* (Å)	*α* (°C)	*β* (°C)	*γ* (°C)	Volume (Å^3)
Phenanthrene	$P2_1$	8.472	6.121	9.402	90	97.92	90	483.0
P_{K1}-1	$P2_1$	7.902	7.623	9.974	90	117.83	90	531.4
P_{K2}-1	$P2_1$	7.706	7.634	10.113	90	109.07	90	562.3
P_{K3}-1	$P2_1$	8.538	7.104	10.660	90	115.71	90	582.6
P_{Al}-1	$P1$	6.537	22.289	3.824	90.33	90.06	83.67	553.8
P_{Ga}-1	$P1$	6.524	22.063	3.842	90.28	90.04	83.68	549.7
P_{In}-1	$P1$	6.263	22.936	3.974	90.00	90.01	84.53	568.2

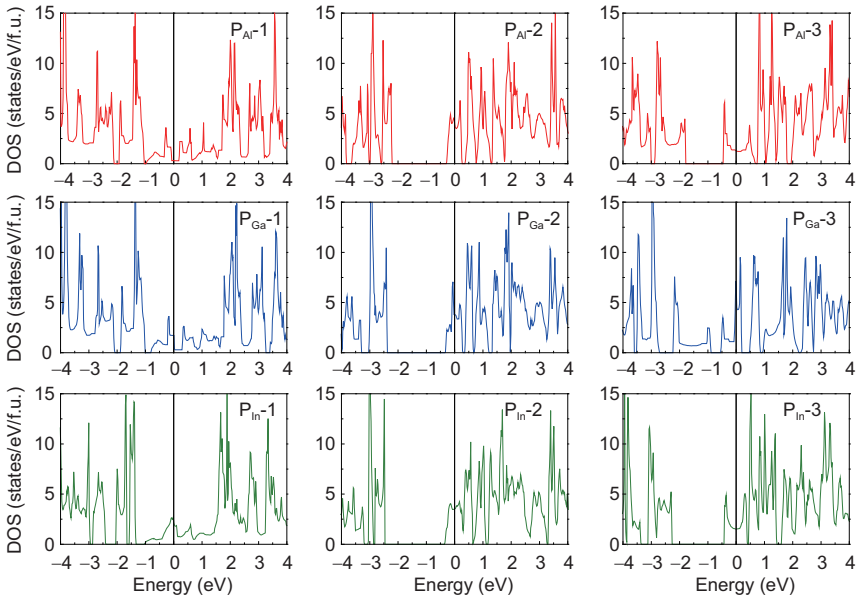

Figure 3 (Color online) Electronic density of states (DOS) of the most stable and metastable structures for Al-/Ga-/In-doped phenanthrene. Zero energy denotes the Fermi level.

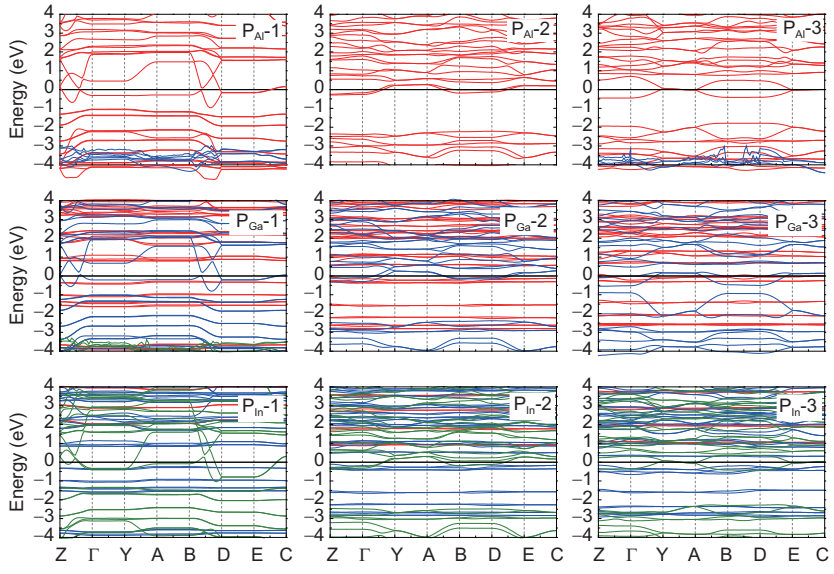

Figure 4 (Color online) Electronic band structures of the most stable and metastable structures for Al-/Ga-/In-doped phenanthrene. Zero energy denotes the Fermi level.

D-*E*-*C* directions, and the Fermi level crosses the bands in both the Z-Γ and *B*-*D* directions. Because of the shortening of the lattice constant in *a*-axis, the band structure of P_{In}-1 shows a visible difference along the *Y*-*A* direction, exhibiting a large dispersion. For some metastable structures, both DOS and band structures have similar characteristics as the K-doped cases because of the same symmetry of $P2_1$, and there are larger DOS values at the Fermi level than for the most stable structures. Focusing on the most stable structures, the DOS value at the Fermi level for $MC_{14}H_{10}$ is relative small compared with $K_3C_{14}H_{10}$ [37]. However, the system exhibits metallic behavior, although no charge transfer occurs in $MC_{14}H_{10}$. Trivalent metal doping is completely different from K doping regarding the electronic properties because of the non-charge transfer-type metal.

By analyzing the fine feature of the stable phase of $MC_{14}H_{10}$ near the Fermi level, we found that all the electronic states at the Fermi level almost come from the valent electrons of *M*. Additionally, the Fermi level does not shift into the conduction bands or valence bands of pristine phenanthrene as K-doped hydrocarbon superconductors [9, 17, 18, 30-32]. The characteristics of the electronic states are similar to the gap states of transition metals or rare earth metal-doped semiconductors [38]. Compared with hydrides chemically precompressed by weight elements [39, 40], the electronic states at the Fermi level in $MC_{14}H_{10}$ do not exhibit a mixture of the electronic characteristics of all elements and the alloy behavior. As a result, we conclude that the metallization of trivalent metal-doped phenanthrene originates from the gap states instead of from charge transfer.

3.3 Superconductivity

Before exploring the superconductivity, we first examined the magnetism of $MC_{14}H_{10}$. Upon setting the non-spin polarization, ferromagnetic spin polarization (FM), and antiferromagnetic spin polarization, their total energies were calculated. $MC_{14}H_{10}$ was stabilized at the non-spin polarization state, namely the nonmagnetic ground state. The total energies of the FM and AFM states were both 2 meV higher than that of the ground state. This result is different from $K_3C_{14}H_{10}$, where it is the AFM ground state [41]. Based on the nonmagnetic property of $MC_{14}H_{10}$, we calculated the electron-phonon interaction and simply evaluated the superconductivity of the system. The electron-phonon coupling constants, λ, of the stable phases of $AlC_{14}H_{10}$, $GaC_{14}H_{10}$, and $InC_{14}H_{10}$ are given by the formula $\lambda = 2\int \frac{\alpha^2F(\omega)}{\omega}d\omega$, and the total λ values of $AlC_{14}H_{10}$, $GaC_{14}H_{10}$, and $InC_{14}H_{10}$ at 3 GPa are 0.32, 0.34, and 0.34, respectively, which means that the electron-phonon interaction is very weak compared with the K-doped cases [42]. However, the logarithmic average of the phonon frequencies, ω_{log}, for $AlC_{14}H_{10}$, $GaC_{14}H_{10}$, and $InC_{14}H_{10}$ at 3 GPa are 1107.2, 1335.6, and 1523.8 K, respectively, which are much larger than the ~ 200 K for the K-doped cases [42]. Based on the obtained ω_{log} and λ, we analyzed the possible superconductivity using the modified McMillan equations from Allen and Dynes [43]

$$T_c = \frac{\omega_{log}}{1.2}\exp\left(-\frac{1.04(1+\lambda)}{\lambda-\mu^*(1+0.62\lambda)}\right), \quad (1)$$

where μ^* is the Coulomb pseudopotential representing the Coulomb repulsion. By selecting the typical $\mu^* = 0.1$, we obtained superconducting transition temperatures of 0.97, 1.91, and 2.18 K for $AlC_{14}H_{10}$, $GaC_{14}H_{10}$, and $InC_{14}H_{10}$ at 3 GPa, respectively, as shown in Figure 5. The calculation results indicate that the trivalent metal-doped phenanthrene may be superconducting. This possible superconductivity of $MC_{14}H_{10}$ is not related to the charge transfer and is weaker than that of K-doped cases. Of course, the superconductivity of *M*-doped phenanthrene still requires further experimental support such as observation of the Meissner effect.

4 Conclusion

In summary, upon trivalent metal Al/Ga/In doping of phenanthrene, we found that there is a great difference in their crystal structures, charge transfer, and electronic properties compared with K-doped phenanthrene. Al/Ga/In doping is not equivalent to three-electron doping in $K_3C_{14}H_{10}$. According to the crystal structure, when Al/Ga/In is doped in phenanthrene, it is difficult for metal atoms to enter the intralayer region; however, it is easier to enter the interlayer region. Moreover, a positive formation energy was obtained, indicating the difficulty of doping Al/Ga/In into phenanthrene. Although the energy band structures of the Al/Ga/In-doped

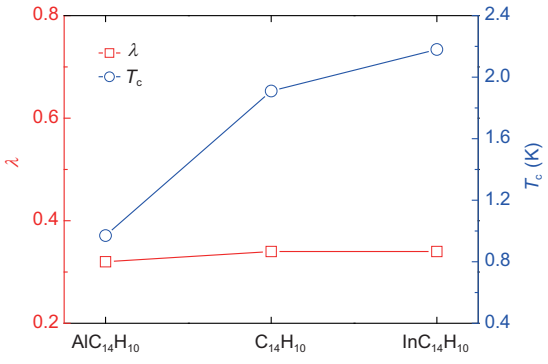

Figure 5 (Color online) Predicted superconducting critical temperature, T_c, and electron-phonon coupling constant, λ, for Al-/Ga-/In-doped phenanthrene.

phenanthrene have two bands that pass through the Fermi level and exhibit a metallic feature, the transferred charge is close to zero, and the metallization is independent of charge transfer. In addition, weak superconductivity caused by the lower DOS value at the Fermi level and weak electron-phonon coupling indicates that Al/Ga/In doping is less effective than K doping. However, the trivalent metal-doped phenanthrene is a possible non-charge transfer superconductor, which will enrich the study of aromatic superconductors, and deepen our understanding of the structure and superconductivity of metal-doped aromatic superconductors.

This work was supported by the Basic Research Program of Shenzhen (Grant Nos. JCYJ20170818153404696, and JCYJ20150925163313898), the National Natural Science Foundation of China Academy of Engineering Physics (Grant No. U1530401), and the National Natural Science Foundation of China (Grant Nos. 11804354, 61574157, and 61774164).

1 V. L. Ginzburg, Phys. Lett. **13**, 101 (1964).
2 W. A. Little, Phys. Rev. **134**, A1416 (1964).
3 V. L. Ginzburg, Sov. Phys. Usp. **19**, 174 (1976).
4 R. Mitsuhashi, Y. Suzuki, Y. Yamanari, H. Mitamura, T. Kambe, N. Ikeda, H. Okamoto, A. Fujiwara, M. Yamaji, N. Kawasaki, Y. Maniwa, and Y. Kubozono, Nature **464**, 76 (2010).
5 Y. Kubozono, H. Mitamura, X. Lee, X. He, Y. Yamanari, Y. Takahashi, Y. Suzuki, Y. Kaji, R. Eguchi, K. Akaike, T. Kambe, H. Okamoto, A. Fujiwara, T. Kato, T. Kosugi, and H. Aoki, Phys. Chem. Chem. Phys. **13**, 16476 (2011).
6 X. F. Wang, R. H. Liu, Z. Gui, Y. L. Xie, Y. J. Yan, J. J. Ying, X. G. Luo, and X. H. Chen, Nat. Commun. **2**, 507 (2011), arXiv: 1102.4075.
7 Q. W. Huang, G. H. Zhong, J. Zhang, X. M. Zhao, C. Zhang, H. Q. Lin, and X. J. Chen, J. Chem. Phys. **140**, 114301 (2014).
8 M. Xue, T. Cao, D. Wang, Y. Wu, H. Yang, X. Dong, J. He, F. Li, and G. F. Chen, Sci. Rep. **2**, 389 (2012).
9 G. H. Zhong, D. Y. Yang, K. Zhang, R. S. Wang, C. Zhang, H. Q. Lin, and X. J. Chen, Phys. Chem. Chem. Phys. **20**, 25217 (2018).
10 R.-S. Wang, Y. Gao, Z.-B. Huang, and X.-J. Chen, arXiv: 1703.05803.
11 R.-S. Wang, Y. Gao, Z.-B. Huang, and X.-J. Chen, arXiv: 1703.05804.
12 R.-S. Wang, Y. Gao, Z.-B. Huang, and X.-J. Chen, arXiv: 1703.06641.
13 H. Li, X. Zhou, S. Parham, T. Nummy, J. Griffith, K. Gordon, E. L. Chronister, and D. D. Dessau, arXiv: 1704.04230.
14 W. Liu, H. Lin, R. Kang, X. Zhu, Y. Zhang, S. Zheng, and H. H. Wen, Phys. Rev. B **96**, 224501 (2017), arXiv: 1706.06018.
15 M. Q. Ren, W. Chen, Q. Liu, C. Chen, Y. J. Qiao, Y. J. Chen, G. Zhou, Z. H. Li, T. Zhang, Y. J. Yan, and D. L. Feng, Phys. Rev. B **99**, 045417 (2019).
16 P. Neha, A. Bhardwaj, V. Sahu, and S. Patnaik, Phys. C-Superconduct. Appl. **554**, 1 (2018), arXiv: 1712.01766.
17 J. F. Yan, G. H. Zhong, R. S. Wang, K. Zhang, H. Q. Lin, and X. J. Chen, J. Phys. Chem. Lett. **10**, 40 (2019).
18 G. Huang, G. H. Zhong, R. S. Wang, J. X. Han, H. Q. Lin, and X. J. Chen, Carbon **143**, 837 (2019).
19 A. F. Hebard, M. J. Rosseinsky, R. C. Haddon, D. W. Murphy, S. H. Glarum, T. T. M. Palstra, A. P. Ramirez, and A. R. Kortan, Nature **350**, 600 (1991).
20 A. Y. Ganin, Y. Takabayashi, Y. Z. Khimyak, S. Margadonna, A. Tamai, M. J. Rosseinsky, and K. Prassides, Nat. Mater. **7**, 367 (2008).
21 D. Jérome, A. Mazaud, M. Ribault, and K. Bechgaard, J. Phyique Lett. **41**, 95 (1980).
22 H. Taniguchi, M. Miyashita, K. Uchiyama, K. Satoh, N. Môri, H. Okamoto, K. Miyagawa, K. Kanoda, M. Hedo, and Y. Uwatoko, J. Phys. Soc. Jpn. **72**, 468 (2003).
23 S. Heguri, Q. Thi Nhu Phan, Y. Tanabe, and K. Tanigaki, Phys. Rev. B **90**, 134519 (2014).
24 Y. Wang, J. Lv, L. Zhu, and Y. Ma, Phys. Rev. B **82**, 094116 (2010), arXiv: 1008.3601.
25 Y. Wang, J. Lv, L. Zhu, and Y. Ma, Comput. Phys. Commun. **183**, 2063 (2012), arXiv: 1205.2264.
26 G. Kresse, and J. Furthmüller, Comput. Mater. Sci. **6**, 15 (1996).
27 G. Kresse, and J. Furthmüller, Phys. Rev. B **54**, 11169 (1996).
28 J. P. Perdew, K. Burke, and M. Ernzerhof, Phys. Rev. Lett. **77**, 3865 (1996).
29 K. Lee, D. Murray, L. Kong, B. I. Lundqvist, and D. C. Langreth, Phys. Rev. B **82**, 081101 (2010), arXiv: 1003.5255.
30 G. H. Zhong, C. Zhang, X. Yan, X. Li, Z. Du, G. Jing, and C. Ma, Mol. Phys. **115**, 472 (2017).
31 X. Wang, G. Zhong, X. Yan, X. Chen, and H. Lin, J. Phys. Chem. Solids **104**, 56 (2017).
32 G. H. Zhong, X. H. Wang, R. S. Wang, J. X. Han, C. Zhang, X. J. Chen, and H. Q. Lin, J. Phys. Chem. C **122**, 3801 (2018).
33 S. Baroni, S. de Gironcoli, A. Dal Corso, and P. Giannozzi, Rev. Mod. Phys. **73**, 515 (2001).
34 N. Troullier, and J. L. Martins, Phys. Rev. B **43**, 1993 (1991).
35 P. Giannozzi, S. Baroni, N. Bonini, M. Calandra, R. Car, C. Cavazzoni, D. Ceresoli, G. L. Chiarotti, M. Cococcioni, I. Dabo, A. Dal Corso, S. de Gironcoli, S. Fabris, G. Fratesi, R. Gebauer, U. Gerstmann, C. Gougoussis, A. Kokalj, M. Lazzeri, L. Martin-Samos, N. Marzari, F. Mauri, R. Mazzarello, S. Paolini, A. Pasquarello, L. Paulatto, C. Sbraccia, S. Scandolo, G. Sclauzero, A. P. Seitsonen, A. Smogunov, P. Umari, and R. M. Wentzcovitch, J. Phys.-Condens. Matter **21**, 395502 (2009), arXiv: 0906.2569.
36 P. Giannozzi, O. Andreussi, T. Brumme, O. Bunau, M. Buongiorno Nardelli, M. Calandra, R. Car, C. Cavazzoni, D. Ceresoli, M. Cococcioni, N. Colonna, I. Carnimeo, A. Dal Corso, S. de Gironcoli, P. Delugas, R. A. DiStasio Jr, A. Ferretti, A. Floris, G. Fratesi, G. Fugallo, R. Gebauer, U. Gerstmann, F. Giustino, T. Gorni, J. Jia, M. Kawamura, H. Y. Ko, A. Kokalj, E. Küçükbenli, M. Lazzeri, M. Marsili, N. Marzari, F. Mauri, N. L. Nguyen, H. V. Nguyen, A. Otero-de-la-Roza, L. Paulatto, S. Poncé, D. Rocca, R. Sabatini, B. Santra, M. Schlipf, A. P. Seitsonen, A. Smogunov, I. Timrov, T. Thonhauser, P. Umari, N. Vast, X. Wu, and S. Baroni, J. Phys.-Condens. Matter **29**, 465901 (2017), arXiv: 1709.10010.
37 X. W. Yan, C. Zhang, G. Zhong, D. Ma, and M. Gao, J. Mater. Chem. C **4**, 11566 (2016).
38 G. Zhong, K. Zhang, F. He, X. Ma, L. Lu, Z. Liu, and C. Yang, Phys. B-Condens. Matter **407**, 3818 (2012).
39 G. Zhong, C. Zhang, X. Chen, Y. Li, R. Zhang, and H. Lin, J. Phys. Chem. C **116**, 5225 (2012).
40 Y. Cheng, C. Zhang, T. Wang, G. Zhong, C. Yang, X. J. Chen, and H. Q. Lin, Sci. Rep. **5**, 16475 (2015).
41 G. Zhong, Z. Huang, and H. Lin, IEEE Trans. Magn. **50**, 1700103 (2014).
42 M. Casula, M. Calandra, G. Profeta, and F. Mauri, Phys. Rev. Lett. **107**, 137006 (2011), arXiv: 1106.1446.
43 P. B. Allen, and R. C. Dynes, Phys. Rev. B **12**, 905 (1975).